Support Vector Regression Models of Reflectarray Unit Cell in a Geometrical 4-D Parallelotope Domain Around a Rectangle of Stability

Daniel R. Prado, Jesús A. López-Fernández and Manuel Arrebola, *Senior Member, IEEE*

***Abstract*—In this work, surrogate models based on support vector regression (SVR) of a multi-resonant unit cell in a geometrical 4-D parallelotope domain are trained and used in a reflectarray antenna design. The multiple sharp resonances of the unit cell prevent a suitable training process in the whole orthotope defined by the available degrees of freedom (DoF). Thus, a strategy to improve the training process and obtain highly accurate models is devised. It consists in defining a parallelotope around a rectangle of stability, which is in turn defined at a lower dimensionality. The SVR models with four geometrical DoF obtained in this parallelotope are shown to provide highly accurate results for the design of a large contoured-beam reflectarray for space applications. The direct optimization with the surrogate models allows to improve the cross-polarization performance several dB while considerably increasing computational performance. Furthermore, compared to lower dimensionality models, the 4-D models offer better results when applied to wideband and dual-band reflectarray direct optimization.**

***Index Terms*—Machine learning, surrogate model, support vector regression (SVR), reflectarray antenna, wideband, dual-band, parallelotope, orthotope**

I. Introduction

MACHINE learning techniques applied to solve complex electromagnetic problems have had a lot of momentum in the past few years [1], [2]. Although there is a wide availability of highly accurate full-wave solvers based on different techniques such as the method of moments (MoM) [3], finite element method [4] or finite-difference time-domain method [5], sometimes they are deemed too slow for design and/or optimization tasks. In the particular case of reflectarray antennas [6] this is specially critical since these antennas are comprised of hundreds or even thousands of unit cells that have to be individually analysed assuming local periodicity (LP) [7]. Thus, achieving a high computational efficiency is an important goal to tackle complex reflectarray designs.

This work was supported in part by the Ministerio de Ciencia, Innovación y Universidades under project IJC2018-035696-I; by MICIN/AEI/10.13039/501100011033 under projects PID2020-114172RB-C21 (ENHANCE-5G) and TED2021-130650B-C22, the last one funded by the NextGenerationEU under the Recovery plan for Europe; by Gobierno del Principado de Asturias under project AYUD/2021/51706.

D. R. Prado, J. A. López-Fernández and M. Arrebola are with the Department of Electrical Engineering, Group of Signal Theory and Communications, Universidad de Oviedo, Gijón, Spain (e-mail: drprado@uniovi.es; jelofer@uniovi.es; arrebola@uniovi.es).

Color versions of one or more of the figures in this paper are available online at http://ieeexplore.ieee.org.

Digital Object Identifier XX.XXXX/TAP.XXXX.XXXXXXX

In this regard, several machine learning techniques have been applied to model the electromagnetic response of reflectarray unit cells, including neural networks [8]–[10], support vector regression (SVR) [11], and ordinary kriging [12], [13]. The goal of using these techniques is to achieve a fast computational performance compared with the use of full-wave solvers while keeping a high degree of accuracy [1]. When applied to the design of reflectarrays at a single frequency, usually only one degree of freedom (DoF) per orthogonal polarization is necessary [6]. Still, advanced optimizations with improved cross-polarization performance may need more DoF [14]. However, when increasing the number of DoF in surrogate models the curse of dimensionality comes into play [1], [15]. Nevertheless, it is feasible to at least save two DoF by considering several surrogate models, one per angle of incidence [15], allowing to increase the number of geometrical DoF that are useful to perform optimizations.

In this work, we show the results of surrogate models of a multi-resonant reflectarray unit cell with several geometrical DoF per polarization [16]. Two geometrical DoF per linear polarization are considered as input variables to each of the SVR models that are trained per angle of incidence using the LIBSVM tool [17]. Due to the sharp resonances introduced by the unit cell, the training process in an orthotope[1] defined by the available DoF, with a physical range close to the cell periodicity, is unsuitable. Thus, a novel strategy to overcome this limitation is proposed. We initially consider a rectangular 2-D domain of stability where the sharp resonances are avoided. Then, we carry out the surrogate model training in a 4-D domain that consists of a parallelotope containing the stability rectangle. The number of training samples and size of the parallelotope are selected so the predicted reflection coefficients show a high degree of accuracy. Finally, the 4-D SVR surrogate models are employed in the design, analysis, and optimization of a very large contoured beam reflectarray antenna for space applications, showing a considerable improvement in the computational performance while keeping a high degree of accuracy with regard to the MoM-LP tool used as reference. Moreover, thanks to the extra DoF, improved results are obtained in wideband and dual-band direct reflectarray optimizations in both in-band copolar gain and polarization purity when compared to using lower dimensional models.

[1] An orthotope is the generalization of the rectangle in N dimensions, while a parallelotope is the generalization in N dimensions of a parallelepiped [18].

Some preliminary results were already presented in [19]. Here, new insights into the characteristics of the parallelotope domain, a generalization of the domain formulation and generation procedure to any reflectarray unit cell, error analysis studies in the training domain, comparison with lower dimensionality models showing the superiority of the proposed training methodology, and new examples of the application of the high dimensionality models are provided.

II. Surrogate Modelling Based on SVR

SVR is based on the application of support vector machines (SVM) [20] to a regression problem. To that end, the training procedure employs a set of N inputs ($\vec{x}_i \in \chi \subseteq \mathbb{R}^L$) and outputs ($\rho_i \in \mathbb{R}$, corresponding to the real or imaginary part of a reflection coefficient of the reflectarray unit cell), denoted as $T = \{\vec{x}_i, \rho_i\}_{i=1,2,\ldots,N}$. The SVR training provides model functions, noted in general as f, that allow to estimate new values of the reflection coefficients for inputs that were not considered in the training process. The number of those regression functions depends on the strategy used. For instance, in this work we use ten of those functions for each angle of incidence and frequency. The real and imaginary parts of each complex coefficient are modelled separately and, due to the achieved precision, the magnitude of the copolar coefficients yields also two extra models. This function takes the form:

$$f(\vec{x}) = b + \sum_{n=1}^{N_s} \alpha_n K(\vec{x}_n, \vec{x}), \tag{1}$$

where $\vec{x} \in \chi$ is the new input; b is the offset; N_s is the number of support vectors; $\alpha_n = \alpha_n^- - \alpha_n^+$ are the differences of the optimal Lagrange multipliers; K is the kernel function; and $\vec{x}_n$ are the support vectors. For this work, the Gaussian kernel function is employed:

$$K(\vec{x}, \vec{x}') = \exp\left(-\gamma \|\vec{x} - \vec{x}'\|^2\right), \tag{2}$$

where γ is a tunable parameter and $\|\cdot\|$ is the Euclidean norm.

The library LibSVM [17] is employed to carry out the training and obtain b, N_s, α_n and $\vec{x}_n$ that are necessary to evaluate (1). LibSVM finds these parameters after the minimization of a regularized risk functional that factors in the empirical errors weighted by a tunable parameter C and the flatness of function f (which is related to the generalization properties of the SVR model [20]). In addition, the empirical errors are accounted for by means of the ϵ-insensitive loss function, which does not consider the regression errors below a given $\epsilon \geq 0$. Thus, each SVR model is tuned by parameters γ, C and ϵ.

In the present work, parameters γ and C for each SVR model are obtained through a process of cross-validation. To that end, set T is divided into three disjoint subsets with N_r samples for training, N_v samples for validation and N_t samples for testing, such that $N = N_r + N_v + N_t$. A grid search in the (γ, C) plane is performed to find the optimal values. For each point in the (γ, C) plane, the cross-validation procedure uses the training set to train the model and the validation set to obtain the model error. The best model obtained in this way is ultimately evaluated with the test set, giving the error

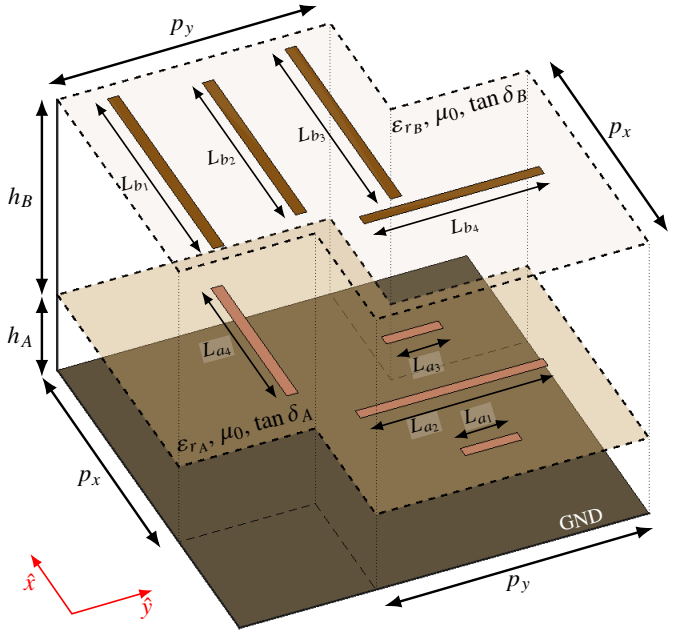

Fig. 1. Sketch of the unit cell employed in this work, with several parallel and coplanar dipoles that provide several degrees of freedom to employ in reflectarray optimization.

of the final selected model. For this process, the following logarithmic relative error in dB is employed:

$$\mathrm{RE} = 20 \log\left(\frac{\|\vec{e}\|}{\|\vec{\rho}\|}\right), \tag{3}$$

where $\vec{\rho} = (\rho_1, \rho_2, \ldots, \rho_M)$ is a vector of M samples of actual outputs, and $\vec{e} = (e_1, e_2, \ldots, e_M)$ with $e_i = \rho_i - f(\vec{x}_i), i = 1, 2, \ldots, M$ is a vector of the difference between the predicted output and the actual output, where f is defined in (1). Moreover, parameter ϵ is dynamically adjusted for each surrogate model depending on the value of the actual outputs as [11]:

$$\epsilon = \sqrt{\frac{3}{N_r}} \sigma_{\mathrm{RE}} \|\vec{\rho}\|, \tag{4}$$

where σ_{RE} is the standard deviation of the relative error in linear scale:

$$\sigma_{\mathrm{RE}} = \sqrt{\mathbb{E}\left\{\frac{\|\vec{e}\|^2}{\|\vec{\rho}\|^2}\right\}} \tag{5}$$

being $\mathbb{E}\{\cdot\}$ the notation for the expected value. σ_{RE} corresponds to the desired error achievable in the asymptotic case ($N_r \to \infty$).

Further details on the SVM background, the grid search on the (γ, C) plane, and the derivation of the expression for ϵ in (4) may be consulted in [11].

III. Definition of a 4-D Parallelotope-Shaped Training Region

In this Section, a methodology for the definition of a 4-D parallelotope-shaped training region is provided. Although the methodology is general, it is detailed with a specific unit cell and subsequently shown how it is applied to other reflectarray elements that offer enough DoF.

A. Unit Cell and Reflectarray Specifications

In this work, the unit cell of Fig. 1 is employed. It consists of four parallel and coplanar dipoles per linear polarization in two layers of metallization. As reference analysis tool, the MoM-LP described in [21] is employed. It will provide the electromagnetic response of the unit cell in the form of four complex reflection coefficients that will be used as outputs in the process of obtaining the SVR models. As inputs, some of the dipole lengths will be employed, keeping constant the rest of the parameters of the unit cell (substrate, dipole widths, etc.). The results shown in the following sections were obtained employing a substrate with $h_A = 2.363\,\text{mm}$ of thickness, $\varepsilon_{r_A} = 2.55$ and $\tan\delta_A = 0.0009$ for the bottom layer, and a substrate with $h_B = 1.5\,\text{mm}$ of thickness, $\varepsilon_{r_B} = 2.17$ and $\tan\delta_B = 0.0009$ for the top layer (see Fig. 1). In addition, the width of the dipoles is 0.5 mm and the separation centre to centre between parallel dipoles is 3.9 mm.

For the practical application of the SVR models, a large reflectarray is considered, comprised of 7052 elements in a regular grid of 86×82 elements and with a feed placed at $(-358, 0, 1070)\,\text{mm}$ with regard to the reflectarray center, generating an average edge illumination taper of $-18.5\,\text{dB}$. The antenna is placed on a satellite in geostationary orbit with a footprint providing European coverage, defined by the French national space agency CNES [22]. The results shown in Sections III, IV, and V were obtained at 11.85 GHz, while multiple frequencies are considered in the direct layout optimizations of Section VI.

B. Degrees of Freedom of the Unit Cell

The dipoles of the unit cell provide a number of resonances that allow to obtain a considerable phase-shift for reflectarray design [3]. However, the relative and absolute lengths of the dipoles, as well as the periodicity, have to be carefully adjusted to avoid sharp resonances, which eventually yield direct coefficients losses, while providing a smooth variation of the phase response [16]. In addition, the appearance of sharp resonances in the SVR training domain may also hamper the training process [23] and eventually increase the error on the surrogate models. Consequently, it is convenient to circumvent sharp resonances as much as possible.

To that end, we start by reducing the eight DoF provided by the lengths of the dipoles to two, named T_x and T_y, by establishing scaling parameters between parallel dipoles. The rationale behind this strategy is to have only one variable per linear polarization (T_x for polarization X and T_y for polarization Y) such that it is easy to prevent resonances in a subset of the (T_x, T_y) plane by tuning the scaling parameters. The relation of T_x and T_y with the dipole lengths of Fig. 1 is:

$$\begin{aligned} &L_{a_1} = \alpha_{a_1} T_y \;;\; L_{a_2} = \alpha_{a_2} T_y \;;\; L_{a_3} = \alpha_{a_3} T_y \;;\; L_{a_4} = \alpha_{a_4} T_x \\ &L_{b_1} = \alpha_{b_1} T_x \;;\; L_{b_2} = \alpha_{b_2} T_x \;;\; L_{b_3} = \alpha_{b_3} T_x \;;\; L_{b_4} = \alpha_{b_4} T_y. \end{aligned} \tag{6}$$

The value of parameters α_{a_i} and α_{b_i}, $i = 1, 2, 3, 4$, must be chosen such that a smooth and large enough variation of the phase-shift is obtained, while sharp resonances are avoided as much as possible. In this respect, we have followed the parametrization suggested in [16], which is summarized next.

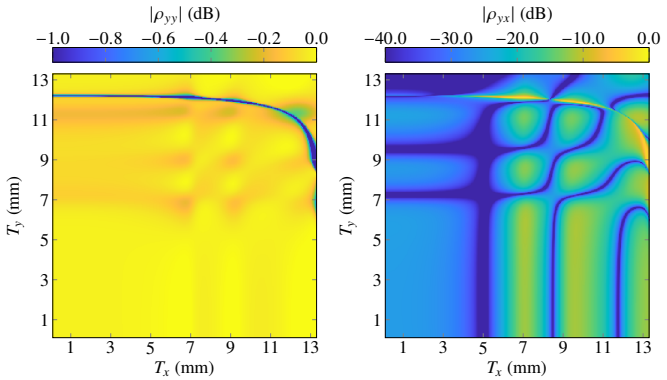

Fig. 2. Magnitude of the (a) direct coefficient ρ_{yy} and (b) cross-coefficient ρ_{yx} in the (T_x, T_y) plane for oblique incidence with $(\theta = 29°, \varphi = 35°)$, a periodicity $p_x = p_y = 14\,\text{mm}$, and $\alpha_{a_1} = \alpha_{a_3} = 0.58$, $\alpha_{a_2} = \alpha_{a_4} = 1$, $\alpha_{b_1} = \alpha_{b_3} = 0.63$, $\alpha_{b_2} = 0.93$, $\alpha_{b_4} = 0.95$.

In the first place, preserving the symmetry of the lateral dipoles, by considering $\alpha_{a_1} = \alpha_{a_3}$ and $\alpha_{b_1} = \alpha_{b_3}$, considerably reduces the cross-polarization of the unit cell. In the second place, a smooth phase response with a sufficiently large range is achieved when using $\alpha_{a_1} = \alpha_{a_3} = 0.58; \alpha_{a_2} = \alpha_{a_4} = 1, \alpha_{b_1} = \alpha_{b_3} = 0.63, \alpha_{b_2} = 0.93; \alpha_{b_4} = 0.95$. Moreover, the periodicity of the unit cell, p_x and p_y, as well as the maximum value that T_x and T_y take must be studied to avoid sharp resonances in the electromagnetic response of the unit cell.

Fig. 2 shows an example for a unit cell with periodicity $p_x = p_y = 14\,\text{mm}$. It plots the magnitude of two reflection coefficients, ρ_{yy} and ρ_{yx}, with $T_x, T_y \in [0.1, 13.3]\,\text{mm}$ to avoid overlap between orthogonal dipoles. For high values of T_x and T_y a sharp resonance appears, which transfers energy from the direct coefficient to the cross-coefficient [24]. These resonances can be avoided by restricting the range of T_x and T_y as well as by reducing the periodicity. In this paper, we use the range $[4, 10]\,\text{mm}$ for both T_x and T_y. This rectangular domain associated to the geometrical features L_{a_2} and L_{a_4} defines (in addition to the selected values of the other parameters α_{a_i} and $\alpha_{b_i}, i = 1, 2, 3, 4$) a stability region, or a rectangle of stability, where the sharp resonances are avoided. In addition, the previously-described procedure to find the rectangle of stability is robust since it depends on several parameters (scaling factors, periodicity and range of T_x and T_y) that offer enough flexibility to establish a good enough stability region.

The use of variables T_x and T_y is enough for designs of dual-polarized reflectarray antennas at a single frequency. However, it is desirable to extend the model to include more geometrical DoF in order to perform advanced reflectarray optimizations [14]. To extend the model to four dimensions, we define the 4-D space $(T_{x_1}, T_{x_2}, T_{y_1}, T_{y_2})$, whose variables are related to the dipole lengths of Fig. 1 as follows:

$$\begin{aligned} &L_{a_1} = \alpha'_{a_1} T_{y_1} \;;\; L_{a_2} = \alpha'_{a_2} T_{y_2} \;;\; L_{a_3} = \alpha'_{a_3} T_{y_1} \;;\; L_{a_4} = \alpha'_{a_4} T_{x_2} \\ &L_{b_1} = \alpha'_{b_1} T_{x_1} \;;\; L_{b_2} = \alpha'_{b_2} T_{x_2} \;;\; L_{b_3} = \alpha'_{b_3} T_{x_1} \;;\; L_{b_4} = \alpha'_{b_4} T_{y_2}. \end{aligned} \tag{7}$$

As in the 2-D case, the variation of the geometrical variables

is restricted to a certain interval. While in the 2-D case this region was a rectangle, in the 4-D case is an orthotope. If we use the same range of variation for the geometrical features in 4-D than in 2-D, we obtain an orthotope that is the fittest one containing the stability rectangle (represented in green color in Fig. 3). The orthogonal projections of this orthotope over the subspaces (T_{x_1}, T_{x_2}) and (T_{y_1}, T_{y_2}) are rectangles that are depicted, with blue color, in Fig. 3(a) and Fig. 3(b), respectively. Assuming that we use the same number of samples for training the SVR in both domains (the 2-D stability rectangle and the fittest 4-D orthotope), the accuracy of the obtained 4-D models is quite low compared to that of the 2-D models. To overcome this lack of accuracy, it is necessary to dramatically increase the number of training samples, which in turn substantially increases the training time, making this approach unappealing.

This is illustrated in Fig. 4, which represents the relative error (in dB) on the real part of the estimated direct coefficient ρ_{xx}, when compared to MoM's, at the stability rectangle for oblique incidence with $(\theta = 29°, \varphi = 35°)$ and a periodicity $p_x = p_y = 12\,\text{mm}$. Fig. 4(a) shows the SVR error when the training domain is the 2-D stability rectangle, which is below $-30\,\text{dB}$ for most of the considered points. Meanwhile, Fig. 4(b) plots the error when the training domain is the 4-D fitted orthotope, which is close to $0\,\text{dB}$ for a non-negligible number of considered points. The mean error over all the data plotted in Fig. 4(a) is $-37.2\,\text{dB}$, while this error is $-16.5\,\text{dB}$ for Fig. 4(b). Similar errors are obtained for other coefficients and angles of incidence.

To increase the accuracy of the 4-D SVR without increasing the number of training points, we suggest performing the training in a parallelotope around the rectangle of stability in the (T_x, T_y) space defined by (6). To that end, we define the parallelotope faces in 4-D by variables $(T_{x_2}, T_{y_2}, \Delta_x, \Delta_y)$ with the following relations:

$$\begin{aligned} T_{x_1} &= \alpha_{b_1} T_{x_2} \pm \Delta_x \\ T_{y_1} &= \alpha_{a_1} T_{y_2} \pm \Delta_y \end{aligned} \tag{8}$$

and:

$$\begin{aligned} \alpha'_{a_1} = \alpha'_{a_3} = 1 \quad ; \quad \alpha'_{a_2} = \alpha_{a_2} \quad ; \quad \alpha'_{a_4} = \alpha_{a_4} \\ \alpha'_{b_1} = \alpha'_{b_3} = 1 \quad ; \quad \alpha'_{b_2} = \alpha_{b_2} \quad ; \quad \alpha'_{b_4} = \alpha_{b_4} \end{aligned} \tag{9}$$

The two new variables Δ_x and Δ_y define, respectively, the size of the parallelotope in the T_{x_1} and T_{y_1} dimensions. In this way, Δ_x and Δ_y allow to control how far from the rectangle of stability the models are trained. Please note that when $\Delta_x = \Delta_y = 0$ the model is reduced to the 2-D case of (6), with $T_{x_2} = T_x$, $T_{y_2} = T_y$, $\alpha_{a_1} = \alpha_{a_3}$ and $\alpha_{b_1} = \alpha_{b_3}$, preserving the symmetry of the lateral dipoles. Fig. 3 shows a representation of different projections of the 4-D parallelotope in 2-D and 3-D subspaces, illustrating, in green color, the rectangle of stability as well.

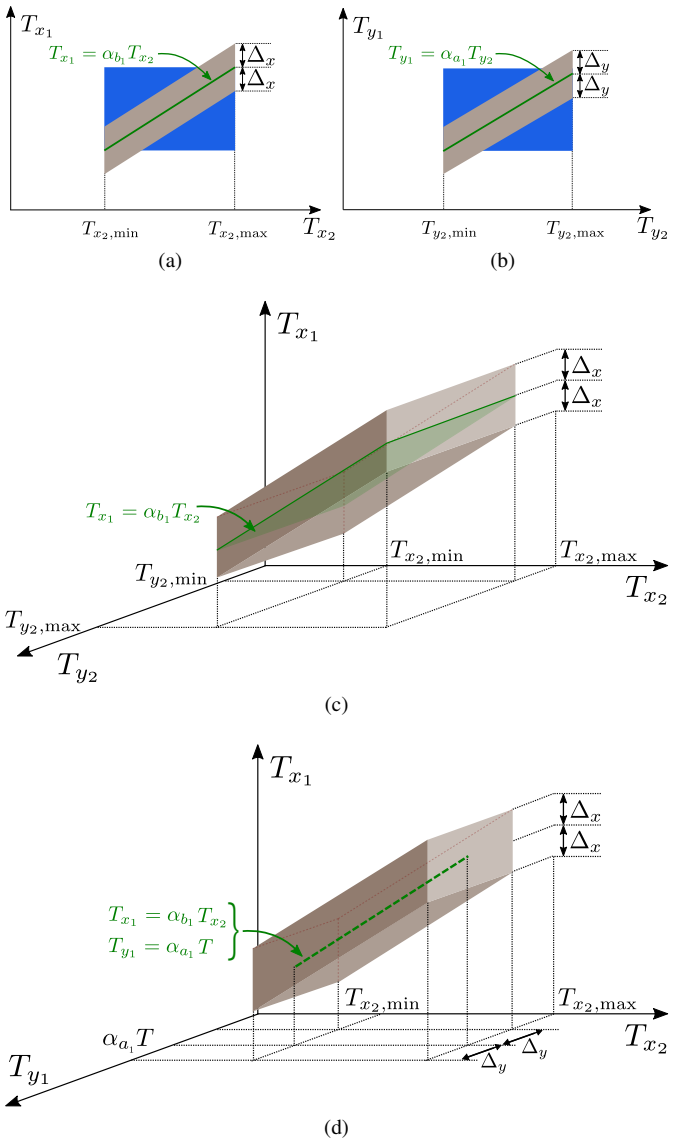

Fig. 3. Low-dimensionality illustration of the region where the SVR models are trained depending on the variables from (7) (in blue) and (8) (in gray). (a) Parallelogram (rectangle) yielded by the orthogonal projection of the parallelotope (orthotope) SVR domain over the (T_{x_1}, T_{x_2}) subspace. (b) Parallelogram (rectangle) produced by the orthogonal projection of the parallelotope (orthotope) SVR domain over the (T_{y_1}, T_{y_2}) subspace. (c) Parallelepiped yielded by the orthogonal projection of the parallelotope SVR domain over the $(T_{x_1}, T_{x_2}, T_{y_2})$ subspace. (d) Parallelepiped that results from the cut of the parallelotope SVR domain along the hyperplane $T_{y_2} = T$. For the sake of clarity, only the orthogonal projections of the fittest orthotope are depicted (beneath the parallelotope projections). In all cases, the stability region is plotted in green.

C. Application to Other Unit Cells

Although the parallelotope has been described for the unit cell shown in Fig. 1, the methodology is general and can be applied to other unit cells that provide several DoF. Indeed, the definition of the parallelotope in (8) depends on four variables, T_{x_2}, T_{y_2}, Δ_x and Δ_y, from which T_{x_1}, T_{y_1} are obtained. As long as a unit cell is able to provide at least four DoF, the same method can be followed to define a 4-D parallelotope where the SVR models may be trained.

As an example, consider a unit cell that comprises two stacked rectangular patches of variable size backed by a ground plane [25]. This unit cell provides a total of four DoF, the width and length of the two rectangular patches, which can be denoted as T_{x_1}, T_{y_1}, T_{x_2} and T_{y_2}. First, the rectangle

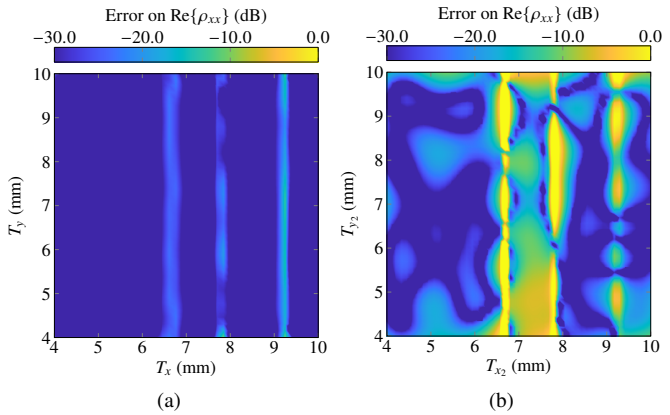

Fig. 4. Relative error in dB of the real part of the estimated direct coefficient ρ_{xx} at the stability rectangle for oblique incidence with ($\theta = 29°, \varphi = 35°$) and a periodicity $p_x = p_y = 12$ mm when the SVR is trained using 2500 random samples placed at (a) the stability rectangle and (b) the most fitted orthotope containing the stability rectangle.

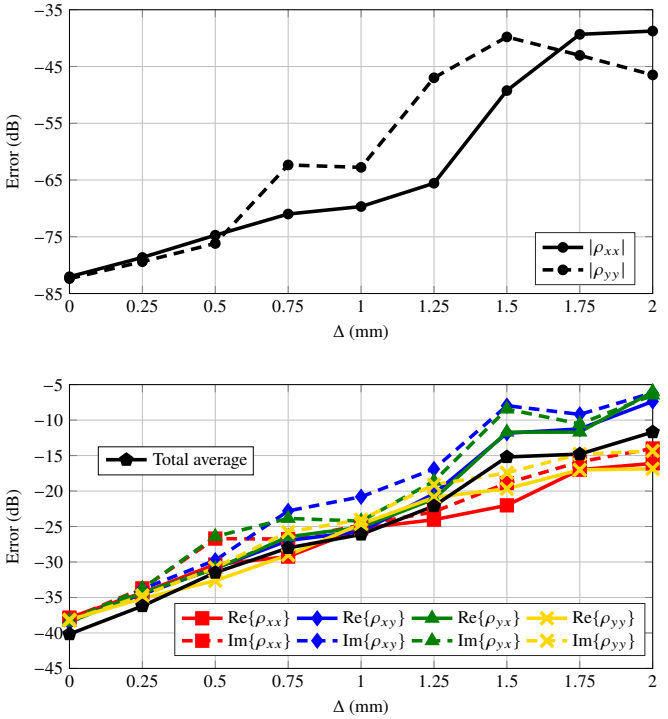

Fig. 5. Relative test error vs. the size of the parallelotope, with $\Delta_x, \Delta_y \in [0, \Delta]$ and $T_{x_2}, T_{y_2} \in [4, 10]$ mm. The total average error also includes the error of the magnitude of the direct coefficients.

of stability in a plane (T_x, T_y) is obtained by finding two suitable scaling factors, α_x and α_y such that $T_x = T_{x_1} = \alpha_x T_{x_2}$ and $T_y = T_{y_1} = \alpha_y T_{y_2}$. Then, the parallelotope is defined by considering two new variables, Δ_x and Δ_y and using (8). In this way, a geometrical 4-D parallelotope has been defined for a different unit cell by following the same procedure described above.

IV. Error Analysis in the Training Domain

A. Error Versus the Size of the Parallelotope

Once the parallelotope region has been defined in (8), it is interesting to analyse how the error of the surrogate models varies with the size of such region. The rectangle of stability is defined for:

$$\Delta_x = \Delta_y = 0, \tag{10}$$

and:

$$\begin{aligned} \alpha_{a_1} = \alpha_{a_3} = 0.58 \quad ; \quad \alpha_{a_2} = \alpha_{a_4} = 1 \\ \alpha_{b_1} = \alpha_{b_3} = 0.63 \quad ; \quad \alpha_{b_2} = 0.93 \quad ; \quad \alpha_{b_4} = 0.95, \end{aligned} \tag{11}$$

in (6). Thus, we will analyse the error when the range of Δ_x and Δ_y varies. Specifically, we consider the range $\Delta_x, \Delta_y \in [0, \Delta]$, with $\Delta = 0, 0.25, \ldots, 2$ mm and $T_{x_2}, T_{y_2} \in [4, 10]$ mm.

To analyse the error, the models will be trained using as input variables T_{x_2}, T_{y_2}, Δ_x, Δ_y as defined in (7), (8), (9) and (11) in the ranges specified above. In addition, the training process consists in an efficient grid search in the plane defined by the SVR parameters based on cross-validation [11]. To that end, a total of $N = 2500$ samples in a random grid are considered, divided into three disjoint sets: $N_r = 1750$ for training, $N_v = 375$ for validation and $N_t = 375$ for test. The samples were obtained employing an in-house MoM-LP based on the formulation of [21]. More details on the training process may be found in [11]. Moreover, models are generated for 152 different angles of incidence (discretization #19 from [26, Table 2]), since the angles of incidence are not considered as input variables to the model. Thus, a total of 380 000 samples were generated to train all SVR models (ten per angle of incidence). An average time of 6 ms is needed to generate each sample in parallel mode in a workstation with two Intel Xeon E5-2650v3 CPU at 2.3 GHz. Thus, less than 40 min were required to obtain all samples.

Fig. 5 shows the evolution of the error with the size of the parallelotope. In particular, it shows the average test error (i.e., the error over the test set) across all considered angles of incidence for the magnitude of the direct reflection coefficients ($|\rho_{xx}|$ and $|\rho_{yy}|$) as well as for the real and imaginary part of all coefficients. It shows an average increase in the test error as the range of the offset variables, Δ_x and Δ_y, increases. As a reference, the total average error for $\Delta = 0.25$ mm is -36 dB, while for $\Delta = 2$ mm is -12 dB, taking into account all reflection coefficients.

Fig. 6 shows the simulation of the real part of cross-coefficient ρ_{yx}, for oblique incidence ($\theta = 29°, \varphi = 35°$), using the MoM-LP tool and the SVR models trained for three different parallelotope sizes (those corresponding to $\Delta = 0.5, 1, 2$ mm). It can be seen how, as the size of the parallelotope increases, part of a resonance is included in the training area. In addition, this resonance is smoothed out by the response predicted by the SVR, partly accounting for the increase in the error shown in Fig. 5. Similar results were obtained for other coefficients and cuts of the 4-D parallelotope. From inspecting Fig. 6, it seems that the analysed coefficient is almost independent of T_{y_1}, at least in the resonance-free region. Nevertheless, there is, in fact, a clear dependence on variable T_{y_1} that is illustrated in Fig. 7. Fig. 7(a) plots the MoM simulation of the real part of ρ_{yx}, for oblique incidence ($\theta = 29°, \varphi = 35°$), over the stability

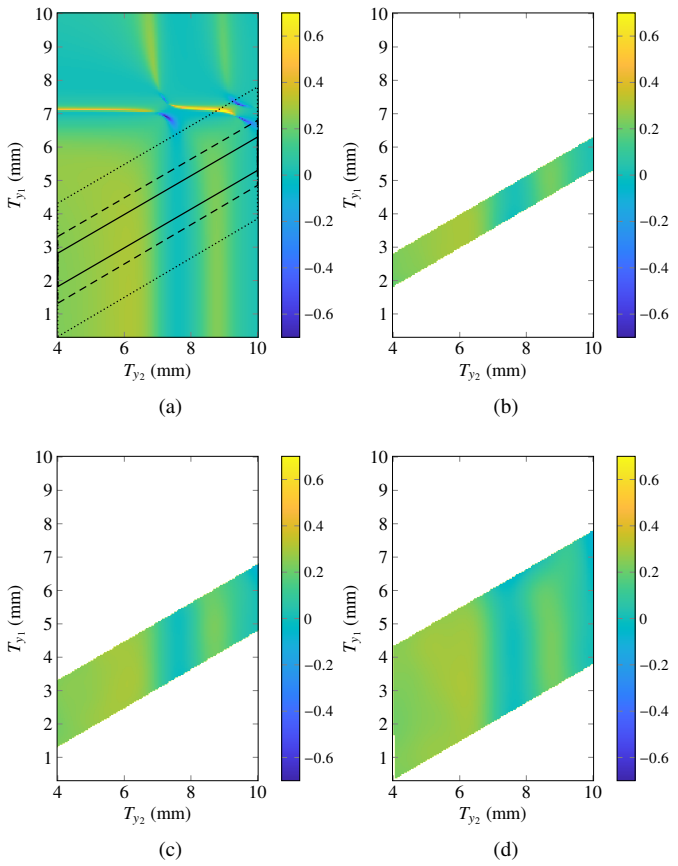

Fig. 6. Simulation of the real part of ρ_{yx} for oblique incidence ($\theta = 29°$, $\varphi = 35°$) using (a) the MoM-LP tool, and SVR models for different parallelotope sizes with (b) $\Delta = 0.5$ mm, (c) $\Delta = 1$ mm, and (d) $\Delta = 2$ mm in the plane (T_{y_2}, T_{y_1}) for $T_{x_1} = 3.9$ mm and $T_{x_2} = 7.1$ mm. The projection of the different parallelotopes is plotted in the top left subfigure for $\Delta = 0.5$ mm (solid), $\Delta = 1$ mm (dashed) and $\Delta = 2$ mm (dotted).

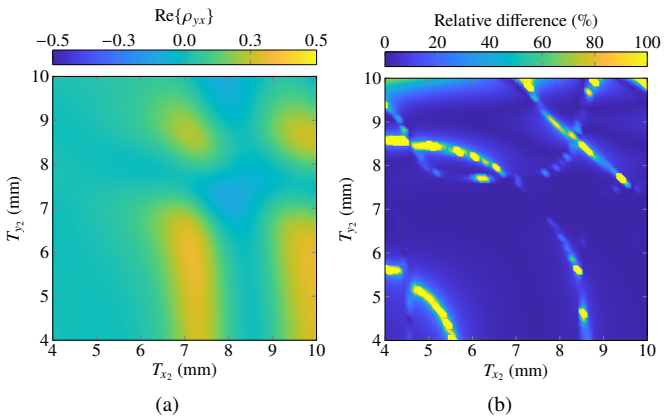

Fig. 7. MoM simulations of the (a) real part of ρ_{yx}, for oblique incidence ($\theta = 29°, \varphi = 35°$), over the stability rectangle and (b) relative difference between the studied coefficient in the stability rectangle and in a rectangle, contained in the parallelotope with size $\Delta = 0.5$ mm, defined by $T_{y_1} = 0.7467\,T_{y_2} - 1.1667$ and $T_{x_1} = 0.63\,T_{x_2}$.

rectangle. Fig. 7(b) depicts the relative difference between the coefficient in Fig. 7(a) and the same one simulated over a rectangle that differs from the stability one just on the relation between T_{y_1} and T_{y_2} that is $T_{y_1} = 0.7467\,T_{y_2} - 1.1667$ (instead of $T_{y_1} = 0.58\,T_{y_2}$). Note that this rectangle is contained in the smallest parallelotope considered in Fig. 6 ($\Delta = 0.5$ mm). Fig. 7(b) shows remarkable relative differences at some areas of the rectangle (T_{x_2}, T_{y_2}) just by varying T_{y_1}.

Based on these results and for comparison purposes, we will select two different 4-D SVR sets of models with a moderately low error for reflectarray analysis and design. The first set, denoted from here on as SVR #1, corresponds to the parallelotope defined by $T_{x_2}, T_{y_2} \in [4, 10]$ mm and $\Delta = 0.5$ mm. These ranges provide an average test error across all models for all reflection coefficients and angles of incidence of -31 dB and a mean training time of 78 s per model following the efficient procedure described in [11]. The second set of models corresponds to $\Delta = 1$ mm (denoted as SVR #2) to test a larger parallelotope, obtaining a mean relative error of -26 dB with a mean training time of 94 s per model. In addition, a 2-D SVR model ($\Delta = 0$ mm) will also be used for comparison purposes when the 4-D SVR models are employed in both a wideband and dual-band reflectarray direct optimization.

B. Error Versus the Number of Training Samples

The relative error shown in Fig. 5 was obtained for a fixed number of training samples, $N_r = 1750$. This number was chosen a posteriori to guarantee a low error of the SVR models. Fig. 8(a) shows the evolution of the average relative test error for all reflection coefficients and angles of incidence for three different sizes of the pallelotope when the number of training samples is varied. As can be seen, as the number of training samples is increased, the average test error decreases, albeit at a slower pace as N_r increases. However, as shown in Fig. 8(b), the average training time per model (using serial processing) shows a meaningful increase with N_r. Thus, there exists a trade-off between the average test error and training time: low errors are achieved at the expense of longer training times and more training samples with diminishing returns. Nevertheless, the training of SVR models can be easily parallelized for each reflection coefficient and angle of incidence, taking advantage of modern multi-processor computers.

In addition, the relative error for the 2-D SVR stagnates early, and the improvement of the error for $N_r > 750$ is negligible. However, this is not the case for the 4-D SVR, whose error has not yet significantly stagnated and could be further reduced by increasing N_r. However, in order to perform a fair comparison between the 2-D and 4-D models, the same number of training samples per angle of incidence will be selected. Furthermore, in order to also guarantee a low test relative error without further increasing the training time, $N_r = 1750$ is selected for subsequent Sections, since it guarantees a low error in both 2-D and 4-D SVR models.

Finally, the computing time shown in Fig. 8(b) does not include the time taken to obtain the training samples (see Section IV-A), which was less than 40 min. However, obtaining the training samples is very efficient with an in-house MoM-LP [21] and it is also a highly parallelizable task.

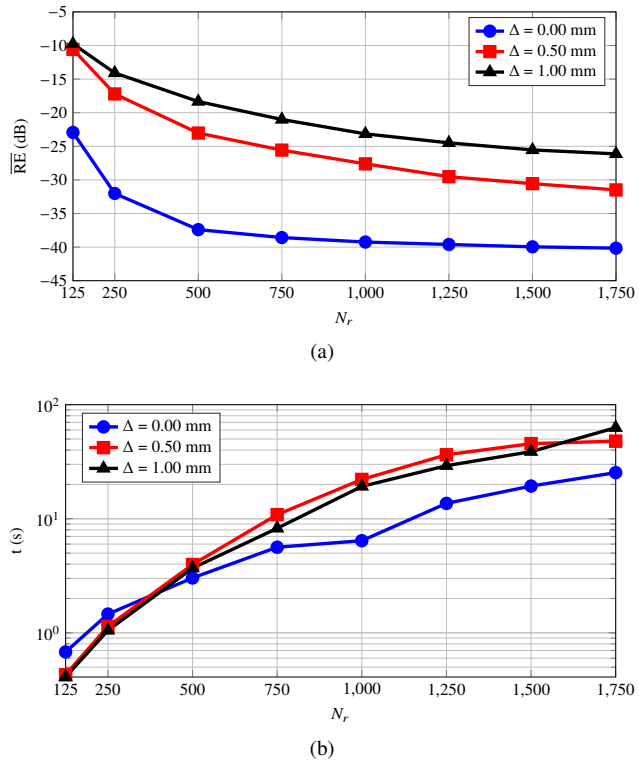

Fig. 8. (a) Average relative test error of the SVR models ($\Delta = 0, 0.5, 1$ mm) and (b) average training time per model versus the number of training samples N_r per angle of incidence.

V. Accuracy of the Models for Layout Design and Reflectarray Analysis

In the case of reflectarray design, an accurate prediction of the phase-shift produced by the direct coefficients is important since it is used to obtain the layout [27]. In this regard, Fig. 9 shows a comparison of the phase and magnitude between MoM-LP simulations and the prediction of the SVR models for the direct coefficient ρ_{xx} and the cross-coefficient ρ_{xy} for oblique incidence ($\theta = 35°, \varphi = 25°$). As can be seen, both SVR models show a high degree of accuracy in both phase and magnitude. In particular, the accuracy in the prediction of the phase-shift allows to perform a dual-linear polarized design by following the procedure detailed in [27] with a mean absolute deviation (MAD) in the obtained layout of only 0.11% for the SVR #1, and a MAD of 0.23% in the case of using the SVR #2. The high accuracy in the layout design can be better seen in Fig. 10, which shows the relative error, for each reflectarray element, of the dipole length L_{a_2} for linear polarization Y with regard to the design carried out with the MoM-LP tool.

In addition, the use of surrogate models accelerate the process of layout design more than two orders of magnitude. While the use of MoM-LP for this task took 2062 seconds using a computer with an Intel i9-9900 at 3.1 GHz, using the SVRs took less than 12 seconds. When a single analysis of the reflectarray is considered, the MoM-LP took an average time of 62 seconds, while the SVR-based analyses took less than 40 milliseconds, giving an acceleration factor larger than three orders of magnitude. In all cases, computations are parallelized, processing one reflectarray element per available thread with OpenMP [28].

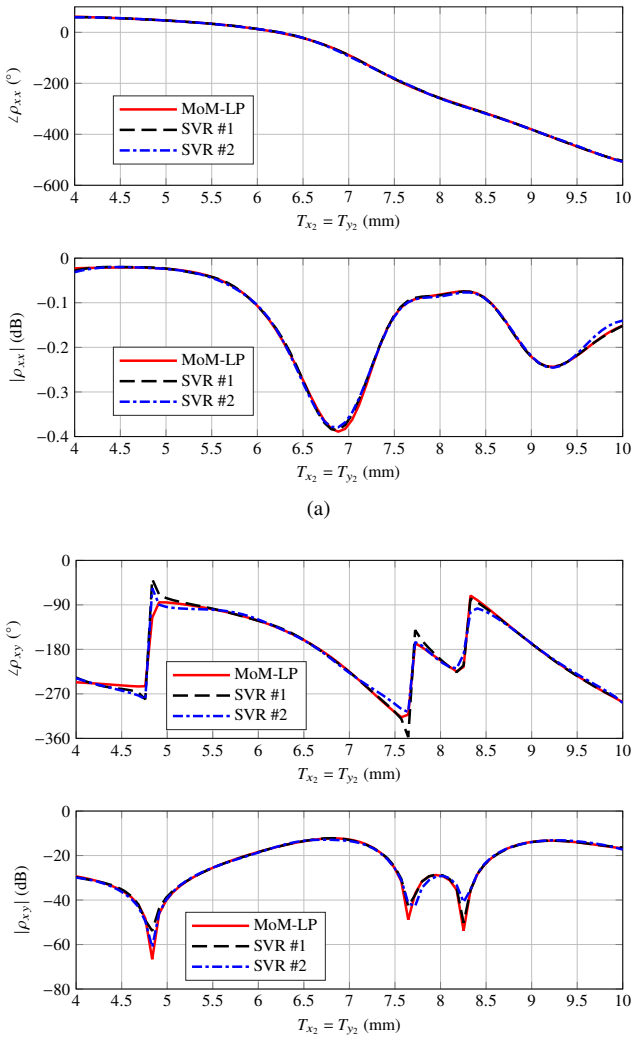

Fig. 9. Comparison of the MoM-LP and SVR simulations of the reflection coefficients (a) ρ_{xx} and (b) ρ_{xy} in phase and magnitude for oblique incidence ($\theta = 35°$, $\varphi = 25°$). Results on the stability rectangle.

When the layout is simulated by the different tools, the radiation pattern shown in Fig. 11 is obtained. As can be seen, both the copolar pattern and the crosspolar discrimination (XPD) show a high degree of accuracy between the different simulation tools. The small discrepancies in the case of the XPD are produced in areas where the crosspolar pattern presents values 40 dB or more lower than the peak copolar gain. Since the accuracy of the SVR models in the prediction of the reflection coefficients and copolar component of the radiation pattern is very high, these small differences in the XPD are partly attributed to the discretization of the angles of incidence [26].

Table I summarizes the results concerning the main figures of merit in the coverage zone. $\mathrm{CP_{min}}$ is the minimum copolar gain, given in dBi; while $\mathrm{XPD_{min}}$ and XPI are the minimum crosspolar discrimination and crosspolar isolation, respectively, and are given in dB. The values of these figures of merit are predicted with a very high degree of accuracy by both SVR models. It is noteworthy that, for the case of the cross-

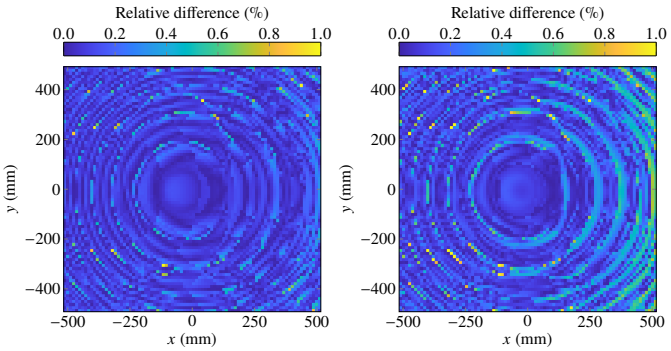

Fig. 10. For the reflectarray layout design, relative error of the dipole length L_{a_2} for linear polarization Y and for each reflectarray element with regard to the design carried out with MoM-LP when employing the (a) SVR #1 and (b) SVR #2.

polarization figures of merit, the largest discrepancy is smaller than 0.4 dB, produced for the XPI in polarization X. These results show the high degree of accuracy achieved with the surrogate models by following the proposed training strategy.

It is worth mentioning that other works comparing 2-D SVR models with MoM-LP have shown a similar degree of accuracy in the prediction of the radiation patterns as the 4-D SVR models presented here [27].

VI. Direct Layout Optimization for Cross-Polarization Performance Improvement

A. Single Frequency Optimization

The main goal of increasing the dimensionality of surrogate models with geometrical features of the unit cell is to use these extra DoF in optimization. Here, a direct layout optimization at a single frequency, 11.85 GHz, will be carried out to improve the cross-polarization figures of merit XPD_{min} and XPI while keeping CP_{min} as high as possible. The optimization will be done in dual-linear polarization. For this task, the generalized intersection approach (GIA) [29] for reflectarray antennas [27] is employed. The starting point for this optimization is the reflectarray layout designed with the SVR #1. Since to obtain this layout only variables T_x and T_y from (6) are employed, the starting value of Δ_x and Δ_y is zero. The optimization will consider four optimizing variables per reflectarray element, T_{x_2}, T_{y_2}, Δ_x and Δ_y. In addition, the optimization must consider the different range of each variable for which the SVR models were trained.

The GIA is run for eight iterations with SVR #1, after which the cross-polarization figures of merit are close to 40 dB, which was the goal set. Table II shows the results of the radiation pattern figures of merit. Both the initial and optimized layout were obtained with the SVR #1. The simulations using the MoM-LP tool with the real angles of incidence are considered the reference. They show an improvement of more than 5 dB of the cross-polarization figures of merit over the initial layout, while maintaining the gain in the coverage area. When compared to the SVR-based simulation, there is a discrepancy of around 1.5 dB for the cross-polarization

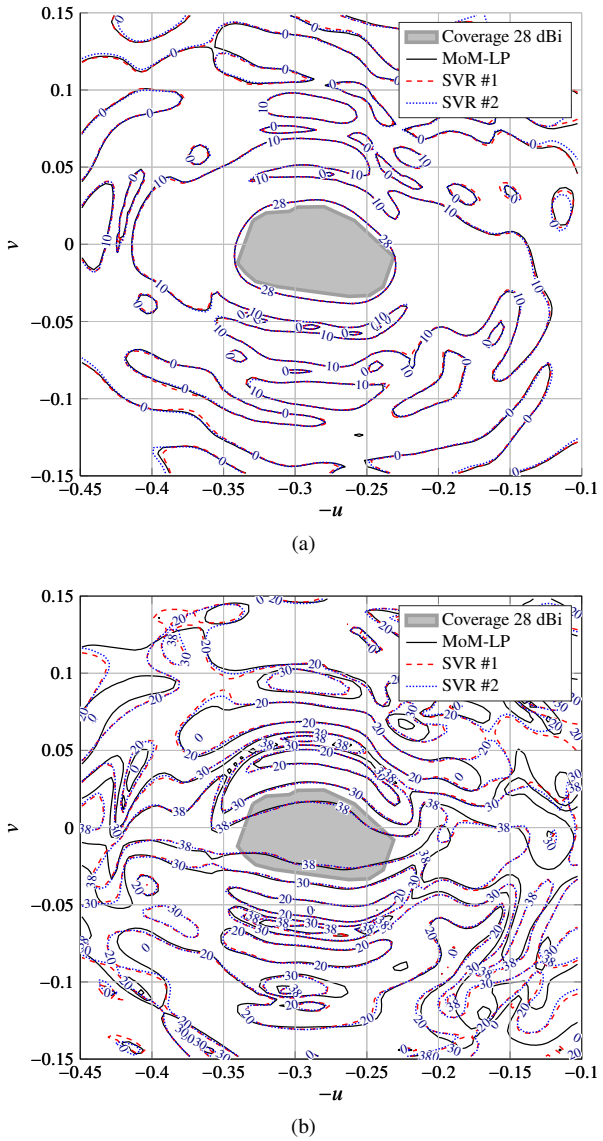

Fig. 11. Comparison of the simulations with MoM-LP, SVR #1 and SVR #2 for the (a) copolar pattern and (b) crosspolar discrimination for polarization X of a reflectarray with European coverage using a layout obtained with SVR #1.

Table I
Figures of merit of a European coverage pattern when the analysis is carried out using different tools. CP_{MIN} is in dBi and XPD_{MIN} and XPI are in dB.

	Polarization X			Polarization Y		
Tool	$\textbf{CP}_{\textbf{min}}$	$\textbf{XPD}_{\textbf{min}}$	**XPI**	$\textbf{CP}_{\textbf{min}}$	$\textbf{XPD}_{\textbf{min}}$	**XPI**
MoM-LP	30.03	32.91	32.86	30.00	32.88	32.82
SVR #1	30.03	32.75	32.53	30.02	32.86	32.82
SVR #2	30.02	32.85	32.64	29.97	32.66	32.61

parameters for both linear polarizations. These differences are partly attributed to small inaccuracies in the SVR model that, along with the very low value of the crosspolar pattern after the optimization procedure, cause larger differences than in the non-optimized layout, as shown in Table I. When the MoM-LP simulation is carried out with the same angular discretization

Table II
FIGURES OF MERIT OF A EUROPEAN COVERAGE PATTERN AFTER THE GIA OPTIMIZATION ALGORITHM IS RUN FOR EIGHT ITERATIONS TO PERFORM A DIRECT LAYOUT OPTIMIZATION TO IMPROVE CROSS-POLARIZATION PERFORMANCE. CP_{MIN} IS IN DBI AND XPD_{MIN} AND XPI ARE IN DB.

Layout	Analysis Tool	θ, φ	Polarization X			Polarization Y		
			CP_{min}	XPD_{min}	XPI	CP_{min}	XPD_{min}	XPI
Initial	MoM-LP	Real	30.03	32.91	32.86	30.00	32.88	32.82
Optimized	MoM-LP	Real	30.04	38.35	38.18	30.01	38.31	38.27
Optimized	MoM-LP	Discretized	30.05	38.70	38.57	30.00	38.83	38.61
Optimized	SVR	Discretized	30.06	39.96	39.76	30.01	39.82	39.54

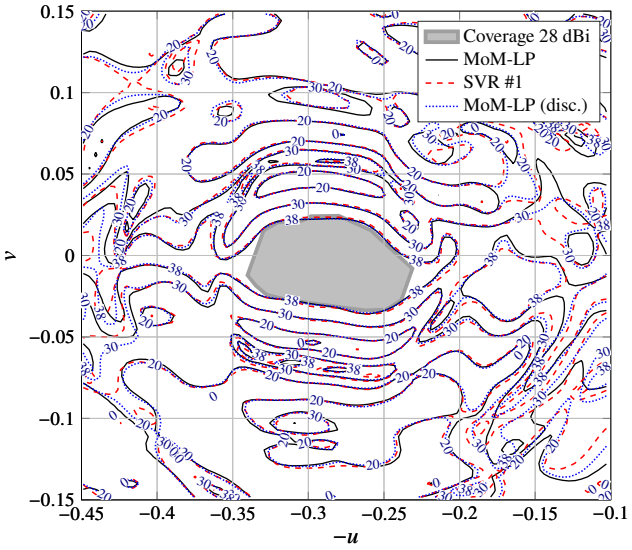

Fig. 12. Comparison of the simulations with MoM-LP and SVR #1 of the XPD for the optimized layout.

used in the SVR models, differences are smaller. Fig. 12 shows the comparison of the simulations with MoM-LP and SVR #1 of the XPD for the optimized layout. The achieved accuracy in the contour lines is comparable to that shown in Fig. 11(b). Similar results were obtained with SVR #2.

B. Multi-Frequency Optimization

To assess the improvement of the 4-D SVR over previous works that employ a 2-D SVR [23], two more optimizations in dual-linear polarization were done. First, a single wideband optimization in the range 10.95 GHz–12.75 GHz (15.2% relative bandwidth) is carried out. This band is divided into five equispaced frequencies at which the optimization is performed. In addition, the feed generates an average illumination taper that varies between −14.8 dB and −25.3 dB in the whole band. Second, a dual-band optimization for a transmit-receive reflectarray is carried out. The transmit band comprises the range 11.70 GHz–12.20 GHz, while the receive band comprises the range 13.75 GHz–14.25 GHz. Furthermore, the feed generates an average illumination taper of −19.4 dB in the transmit band, and of −26.2 dB in the receive band.

For both optimizations, two different SVR are considered. On the one hand, a 2-D SVR is employed. This SVR model is obtained by simply considering a parallelotope with $\Delta = 0$ mm, since in this case $\Delta_x = \Delta_y = 0$ and the domain is reduced to the rectangle of stability. On the other hand, for the 4-D SVR we use SVR #1 ($\Delta = 0.5$ mm). The starting layout for both multi-frequency optimizations is the layout that radiates the European coverage obtained with SVR #1 in Section V. The goal is to achieve a minimum copolar gain of 28 dBi [22] and maximize the cross-polarization performance.

Tables III and IV show the results for the single wideband and dual-band optimizations, respectively. For each frequency, the worst result between both linear polarizations is shown. Although the optimizations were carried out with the SVR models, the results shown in both Tables were obtained after simulating the final optimized layouts with a MoM-LP. Since the initial layout was obtained at 11.85 GHz, its performance at frequencies close to the design one is relatively good. However, performance quickly deteriorates as the frequency is shifted away from 11.85 GHz. After the optimization with the 2-D SVR, both copolar and cross-polarization performances are improved across all frequencies. However, the minimum copolar gain does not comply with the goal of 28 dBi. These results are consistent with the ones obtained with the 2-D SVR in previous works [23]. The 4-D SVR provides extra DoF to improve the performance of the antenna. Indeed, in addition to improving the copolar gain, complying with the goal of achieving at least 28 dBi at all frequencies, cross-polarization performance is further improved, showing how the 4-D SVR provides an edge when compared to the 2-D SVR for wideband and dual-band reflectarray direct optimization.

Finally, Fig. 13 shows the synthesized layout of the dual-band reflectarray top layer obtained with the 4-D SVR.

C. Computational Performance Improvement

Regarding computational performance of the GIA, the direct layout optimization considered four DoF per reflectarray element, thus having in total 28 208 optimizing variables. A short instance of the GIA was run with the MoM-LP at a single frequency for comparison purposes. The mean time per iteration when using MoM-LP is 243.5 s, while it is 64.8 s when using SVR #1. The main building blocks accelerated by the use of surrogate models is the computation of the cost function, which goes from 36.7 s using MoM-LP to 0.04 s using SVR, an acceleration factor of three orders of magnitude; and the calculation of the Jacobian matrix, which goes from 147.3 s down to 9.2 s, more than one order of magnitude faster.

Table III
FIGURES OF MERIT OF A EUROPE COVERAGE AFTER A WIDEBAND OPTIMIZATION AT FIVE DIFFERENT FREQUENCIES WITH A 2-D SVR ($\Delta = 0$ mm) AND A 4-D SVR ($\Delta = 0.5$ mm). OPTIMIZED LAYOUTS WERE SIMULATED WITH MOM-LP. ΔCP_{MIN} IS THE DIFFERENCE BETWEEN THE ACHIEVED MINIMUM GAIN AND THE GOAL OF 28 DBI IN THE COVERAGE AREA. ΔCP_{MIN} AND XPI ARE IN DB.

	10.95 GHz		**11.40 GHz**		**11.85 GHz**		**12.30 GHz**		**12.75 GHz**	
	ΔCP_{min}	**XPI**	**ΔCP_{min}**	**XPI**	**ΔCP_{min}**	**XPI**	**ΔCP_{min}**	**XPI**	**ΔCP_{min}**	**XPI**
Initial layout	−4.62	25.86	0.23	30.06	1.89	32.25	−1.22	29.01	−5.65	23.85
Opt. SVR 2D	−0.70	31.95	1.07	34.86	1.36	35.79	1.06	35.70	−0.07	34.47
Opt. SVR 4D	0.09	38.48	0.59	39.25	0.95	39.73	0.64	39.21	0.19	38.54

Table IV
FIGURES OF MERIT OF A EUROPE COVERAGE AFTER A DUAL-BAND OPTIMIZATION AT SIX DIFFERENT FREQUENCIES WITH A 2-D SVR ($\Delta = 0$ mm) AND A 4-D SVR ($\Delta = 0.5$ mm). TRANSMIT BAND IS 11.70 GHZ–12.20 GHZ, AND RECEIVE BAND IS 13.75 GHZ–14.25 GHZ. OPTIMIZED LAYOUTS WERE SIMULATED WITH MOM-LP. ΔCP_{MIN} IS THE DIFFERENCE BETWEEN THE ACHIEVED MINIMUM GAIN AND THE GOAL OF 28 DBI IN THE COVERAGE AREA. ΔCP_{MIN} AND XPI ARE IN DB.

	11.70 GHz		**11.95 GHz**		**12.20 GHz**		**13.75 GHz**		**14.00 GHz**		**14.25 GHz**	
	ΔCP_{min}	**XPI**	**ΔCP_{min}**	**XPI**	**ΔCP_{min}**	**XPI**	**ΔCP_{min}**	**XPI**	**ΔCP_{min}**	**XPI**	**ΔCP_{min}**	**XPI**
Initial layout	1.69	32.21	1.82	31.25	−1.60	29.00	−14.71	11.57	−4.36	−6.20	−25.87	0.34
Opt. SVR 2D	0.59	32.94	1.91	33.98	0.68	34.36	−0.09	31.63	−0.25	30.32	−1.81	26.66
Opt. SVR 4D	0.10	38.59	1.64	40.26	0.88	39.69	0.58	38.44	0.51	36.98	0.04	35.19

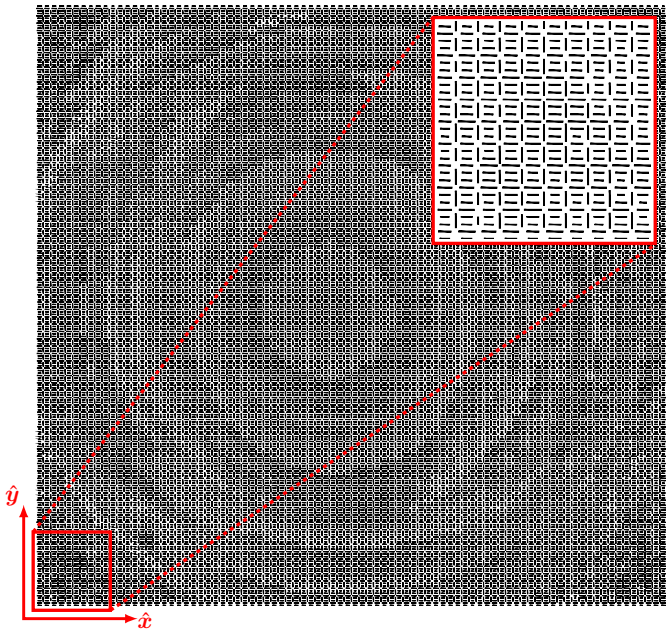

Fig. 13. Mask layout of the top layer of the optimized dual-band reflectarray with European coverage obtained with SVR #1.

However, the rest of the computationally heavy operations in the GIA are not sped-up by the use of machine learning algorithms, including matrix-matrix multiplications and the linear equation solver. Still, the time gains in whole optimization processes may be substantial when multiple stages comprised of many iterations are involved, and these gains are larger when multi-frequency optimizations are carried out. For the case in which the optimization is carried out at five different frequencies, the average time per iteration goes from 1060.8 s with the MoM-LP to 133.1 s with SVR #1. Thus the average speed-up factor of using SVR instead of MoM-LP goes from 3.76 (64.8 s instead of 243.5 s, or 178.7 s of time saved per iteration) at a single frequency to 7.97 (133.1 s instead of 1060.8 s, or 927.7 s of time saved per iteration) when optimizing at five different frequencies, as it is the case of the wideband optimization whose results are shown in Table III. These computational time savings show another advantage of the presented technique in the context of wideband or dual-band optimization compared to the monochromatic case.

VII. CONCLUSION

A novel general strategy to train surrogate models based on SVR on a 4-D geometrical parallelotope domain has been presented. The model solely uses geometrical features as input variables since only those are used in direct layout optimizations. Consequently, each angle of incidence associates a different surrogate model. Since the model training within the 4-D orthotope, defined by the original geometrical features ranges, yields a dramatical decrease on their accuracy compared to the one obtained on the 2-D models, the model training is carried out in a parallelotope around a rectangle of stability without sharp resonances. Results show a high degree of accuracy between the SVR models and the reference MoM-LP simulations in design, reflectarray analysis, and direct layout optimization for cross-polarization improvement. Moreover, when compared with lower dimensionality models employed in previous works, the new 4-D SVR models yield better results in both wideband and dual-band reflectarray direct optimizations. In addition, the use of these surrogate models allows to considerably speed up the analysis, layout design, and direct layout optimization. Specifically, they are accelerated more than three, two, and one orders of magnitude respectively, while keeping a high degree of accuracy with regard to the MoM-LP tool. Finally, the proposed methodology

to train surrogate models in a 4-D geometrical parallelotope domain can also be used with other machine learning algorithms such as artificial neural networks and ordinary kriging.

ACKNOWLEDGMENT

The authors would like to thank Dr. R. Florencio, Prof. R. R. Boix and Prof. J. A. Encinar for providing the MoM-LP software; and Prof. Chih-Chung Chang and Prof. Chih-Jen Lin for making freely available the LIBSVM software.

REFERENCES

[1] A. Massa, G. Oliveri, M. Salucci, N. Anselmi, and P. Rocca, "Learning-by-examples techniques as applied to electromagnetics," *J. Electromagn. Waves Appl.*, vol. 32, no. 4, pp. 516–541, 2018.

[2] A. Massa, D. Marcantonio, X. Chen, M. Li, and M. Salucci, "DNNs as applied to electromagnetics, antennas, and propagation—A review," *IEEE Antennas Wireless Propag. Lett.*, vol. 18, no. 11, pp. 2225–2229, 2019.

[3] R. Florencio, R. R. Boix, J. A. Encinar, and G. Toso, "Optimized periodic MoM for the analysis and design of dual polarization multilayered reflectarray antennas made of dipoles," *IEEE Trans. Antennas Propag.*, vol. 65, no. 7, pp. 3623–3637, Jul. 2017.

[4] V. de la Rubia, J. Zapata, and M. A. González, "Finite element analysis of periodic structures without constrained meshes," *IEEE Trans. Antennas Propag.*, vol. 56, no. 9, pp. 3020–3028, Sep. 2008.

[5] E. Girard, R. Moulinet, R. Gillard, and H. Legay, "An FDTD optimization of a circularly polarized reflectarray unit cell," in *IEEE Antennas and Propagation Society International Symposium*, vol. 3, San Antonio, Texas, USA, Jun. 16–21, 2002, pp. 136–139.

[6] J. Huang and J. A. Encinar, *Reflectarray Antennas*. Hoboken, NJ, USA: John Wiley & Sons, 2008.

[7] D. M. Pozar, S. D. Targonski, and R. Pokuls, "A shaped-beam microstrip patch reflectarray," *IEEE Trans. Antennas Propag.*, vol. 47, no. 7, pp. 1167–1173, Jul. 1999.

[8] L. Shi, Q. Zhang, S. Zhang, C. Yi, and G. Liu, "Efficient graphene reconfigurable reflectarray antenna electromagnetic response prediction using deep learning," *IEEE Access*, vol. 9, pp. 22 671–22 678, Jan. 2021.

[9] P. Robustillo, J. Zapata, J. A. Encinar, and J. Rubio, "ANN characterization of multi-layer reflectarray elements for contoured-beam space antennas in the Ku-band," *IEEE Trans. Antennas Propag.*, vol. 60, no. 7, pp. 3205–3214, Jul. 2012.

[10] A. Çalışkan and F. Güneş, "3D EM data-driven artificial network-based design optimization of circular reflectarray antenna with semi-elliptic rings for X-band applications," *Microw. Opt. Technol. Lett.*, 2022, early access.

[11] D. R. Prado, J. A. López-Fernández, G. Barquero, M. Arrebola, and F. Las-Heras, "Fast and accurate modeling of dual-polarized reflectarray unit cells using support vector machines," *IEEE Trans. Antennas Propag.*, vol. 66, no. 3, pp. 1258–1270, Mar. 2018.

[12] M. Salucci, L. Tenuti, G. Oliveri, and A. Massa, "Efficient prediction of the EM response of reflectarray antenna elements by an advanced statistical learning method," *IEEE Trans. Antennas Propag.*, vol. 66, no. 8, pp. 3995–4007, Aug. 2018.

[13] G. Oliveri, M. Salucci, and A. Massa, "Towards efficient reflectarray digital twins - an EM-driven machine learning perspective," *IEEE Trans. Antennas Propag.*, 2022, early access.

[14] D. R. Prado, M. Arrebola, M. R. Pino, and G. Goussetis, "Contoured-beam dual-band dual-linear polarized reflectarray design using a multi-objective multi-stage optimization," *IEEE Trans. Antennas Propag.*, vol. 68, no. 11, pp. 7682–7687, Nov. 2020.

[15] D. R. Prado, J. A. López-Fernández, M. Arrebola, and G. Goussetis, "On the use of the angle of incidence in support vector regression surrogate models for practical reflectarray design," *IEEE Trans. Antennas Propag.*, vol. 69, no. 3, pp. 1787–1792, Mar. 2021.

[16] R. Florencio, J. A. Encinar, R. R. Boix, V. Losada, and G. Toso, "Reflectarray antennas for dual polarization and broadband telecom satellite applications," *IEEE Trans. Antennas Propag.*, vol. 63, no. 4, pp. 1234–1246, Apr. 2015.

[17] C.-C. Chang and C.-J. Lin, "LIBSVM: A library for support vector machines," *ACM Trans. Intell. Syst. Technol.*, vol. 2, no. 3, pp. 27:1–27:27, Apr. 2011, software available at https://www.csie.ntu.edu.tw/~cjlin/libsvm.

[18] H. S. M. Coxeter, *Regular Polytopes*. London, UK: Methuen & Co. Ltd., 1948.

[19] D. R. Prado, J. A. López-Fernández, and M. Arrebola, "Reflectarray antenna direct optimization using surrogate models with several geometrical degrees of freedom per polarization," in *IEEE MTT-S International Conference on Numerical Electromagnetic and Multiphysics Modeling and Optimization (NEMO)*, Limoges, France, Jul. 6–8, 2022, pp. 1–4.

[20] V. Vapnik, *The Nature of Statistical Learning Theory*, 2nd ed. New York, NY, USA: Springer, 1999.

[21] R. Florencio, R. R. Boix, and J. A. Encinar, "Enhanced MoM analysis of the scattering by periodic strip gratings in multilayered substrates," *IEEE Trans. Antennas Propag.*, vol. 61, no. 10, pp. 5088–5099, Oct. 2013.

[22] J. A. Encinar, M. Arrebola, M. Dejus, and C. Jouve, "Design of a 1-metre reflectarray for DBS application with 15% bandwidth," in *First European Conference on Antennas and Propagation (EuCAP)*, Nice, France, Nov. 6–10, 2006, pp. 1–5.

[23] D. R. Prado, J. A. López-Fernández, M. Arrebola, M. R. Pino, and G. Goussetis, "Wideband shaped-beam reflectarray design using support vector regression analysis," *IEEE Antennas Wireless Propag. Lett.*, vol. 18, no. 11, pp. 2287–2291, Nov. 2019.

[24] J. A. Encinar, M. A. Salas-Natera, M. Barba, M. Arrebola, D. R. Prado, R. R. Boix, and R. Florencio, "Reflectarray antennas with improved performances and design techniques. Final report," European Space Agency, Tech. Rep., Jun. 2016.

[25] J. A. Encinar, "Design of two-layer printed reflectarrays using patches of variable size," *IEEE Trans. Antennas Propag.*, vol. 49, no. 10, pp. 1403–1410, Oct. 2001.

[26] D. R. Prado, J. A. López-Fernández, and M. Arrebola, "Systematic study of the influence of the angle of incidence discretization in reflectarray analysis to improve support vector regression surrogate models," *Electronics*, vol. 9, no. 12, pp. 1–18, Dec. 2020.

[27] D. R. Prado, J. A. López-Fernández, M. Arrebola, and G. Goussetis, "Support vector regression to accelerate design and crosspolar optimization of shaped-beam reflectarray antennas for space applications," *IEEE Trans. Antennas Propag.*, vol. 67, pp. 1659–1668, Mar. 2019.

[28] M. Sato, "OpenMP: parallel programming API for shared memory multiprocessors and on-chip multiprocessors," in *15th International Symposium on System Synthesis*, Kyoto, Japan, Oct. 2–4, 2002, pp. 109–111.

[29] O. M. Bucci, G. D'Elia, G. Mazzarella, and G. Panariello, "Antenna pattern synthesis: a new general approach," *Proc. IEEE*, vol. 82, no. 3, pp. 358–371, Mar. 1994.

Daniel R. Prado was born in Sama de Langreo, Asturias, Spain, in 1986. He received the B.Sc., M.Sc., and Ph.D. degrees in telecommunication engineering from the University of Oviedo, Gijón, Spain, in 2011, 2012, and 2016, respectively.

From 2010 to 2011, he was with The Institute of Electronics, Communications and Information Technology, Queen's University Belfast, Belfast, U.K., where he was involved in the design of leaky-wave antennas as part of his B.Sc. research project. From 2011 to 2017, he was a Research Assistant with the Signal Theory and Communications Area, University of Oviedo, where he was involved in the development of efficient techniques for the analysis and synthesis of reflectarray antennas. In 2014, he was with the School of Electrical Engineering, KTH Royal Institute of Technology, Stockholm, Sweden, as a Visiting Scholar, where he was involved in transformation optics applied to dielectric lenses. From 2018 to 2019, he was with the Institute of Sensors, Signals and Systems, Heriot-Watt University, Edinburgh, U.K. Since 2020 he has been with the Signal Theory and Communications Area, University of Oviedo, as a Post-doctoral researcher. His current research interests include the analysis of uniform and nonuniform arrays, and the development of efficient techniques for the analysis and optimization of near and far fields of spatially-fed antennas, including reflectarrays and transmitarrays.

Dr. Prado was a recipient of a Pre-doctoral Scholarship financed by the Gobierno del Principado de Asturias, a Post-doctoral Fellowship partially financed by the European Union and a Post-doctoral Fellowship financed by the Spanish Government.

Jesús Alberto López-Fernández was born in Avilés, Asturias, Spain. He received the M.Sc. and Ph.D. degrees in telecommunication engineering from the University of Vigo, Vigo, Spain, in 1999 and 2009, respectively.

From April 2002 to March 2003, he was a Marie-Curie Visiting Fellow with the Mechanical & Manufacturing Engineering Department, Trinity College Dublin. Since October 2003, he has been with the Electrical Engineering Department, University of Oviedo, Asturias, Spain, where he is currently an Associate Professor teaching courses on digital communications and radar systems. His current research interests include iterative methods and speed-up schemes, parallel algorithms, machine learning and signal processing.

Manuel Arrebola (Senior Member, IEEE) was born in Lucena, Spain. He received the M.Sc. degree in telecommunication engineering from the University of Málaga, Málaga, Spain, in 2002, and the Ph.D. degree from the Technical University of Madrid (UPM), Madrid, Spain, in 2008.

From 2003 to 2007, he was a Research Assistant with the Department of Electromagnetism and Circuit Theory, UPM. In 2005, he was a Visiting Scholar with the Department of Microwave Techniques, Universität Ulm, Ulm, Germany. In 2007, he joined the Department of Electrical Engineering, University of Oviedo at Gijón, Spain, where he is currently an Associate Professor. In 2009, he was with the European Space Research and Technology Centre, European Space Agency, Noordwijk, The Netherlands, for a period of two months. In 2018, he was a Visiting Professor with the Edward S. Rogers Sr. Department of Electrical and Computer Engineering, University of Toronto, Toronto, ON, Canada. In 2019, he was a Visiting Professor with the Institute of Sensors, Signals and Systems, Heriot-Watt University, Edinburgh, U.K. His current research interests include the application of innovative manufacturing techniques in antenna design, and the development of efficient analysis, design, and optimization techniques of spatial fed arrays and periodic structures for near- and far-field applications.

Dr. Arrebola was a co-recipient of the 2007 Sergei A. Schelkunoff Transactions Prize Paper Award from the IEEE Antennas and Propagation Society. Since 2022, he has been an Associate Editor of the IEEE TRANSACTIONS ON ANTENNAS AND PROPAGATION.